NANO LETTERS

Letter

Crystalline-Amorphous Core#Shell Silicon Nanowires for High Capacity and High Current Battery Electrodes

Li-Feng Cui, Riccardo Ruffo, Candace K. Chan, Hailin Peng, and Yi Cui

Nano Lett., **Article ASAP** • DOI: 10.1021/nl8036323

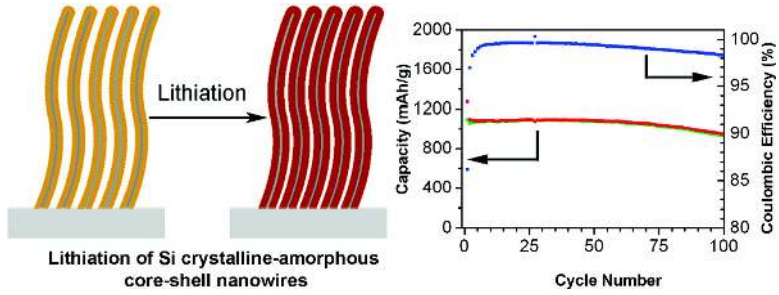

More About This Article

Additional resources and features associated with this article are available within the HTML version:

- Supporting Information
- Access to high resolution figures
- Links to articles and content related to this article
- Copyright permission to reproduce figures and/or text from this article

View the Full Text HTML

Nano Letters is published by the American Chemical Society. 1155 Sixteenth Street N.W., Washington, DC 20036

NANO LETTERS

XXXX
Vol. xx, No. x
-

Crystalline-Amorphous Core−Shell Silicon Nanowires for High Capacity and High Current Battery Electrodes

Li-Feng Cui,[†] Riccardo Ruffo,[‡] Candace K. Chan,[§] Hailin Peng,[†] and Yi Cui*[,†]

Department of Materials Science and Engineering, Department of Chemistry, Stanford University, Stanford, California 94305, and Dipartimento di Scienza dei Materiali, Università degli Studi di Milano-Bicocca, via Cozzi 53, 20135 Milan, Italy

Received December 1, 2008

ABSTRACT

Silicon is an attractive alloy-type anode material for lithium ion batteries because of its highest known capacity (4200 mAh/g). However silicon's large volume change upon lithium insertion and extraction, which causes pulverization and capacity fading, has limited its applications. Designing nanoscale hierarchical structures is a novel approach to address the issues associated with the large volume changes. In this letter, we introduce a core−shell design of silicon nanowires for highpower and long-life lithium battery electrodes. Silicon crystalline-amorphous core−shell nanowires were grown directly on stainless steel current collectors by a simple one-step synthesis. Amorphous Si shells instead of crystalline Si cores can be selected to be electrochemically active due to the difference of their lithiation potentials. Therefore, crystalline Si cores function as a stable mechanical support and an efficient electrical conducting pathway while amorphous shells store Li^+ ions. We demonstrate here that these core−shell nanowires have high charge storage capacity (∼1000 mAh/g, 3 times of carbon) with ∼90% capacity retention over 100 cycles. They also show excellent electrochemical performance at high rate charging and discharging (6.8 A/g, ∼20 times of carbon at 1 h rate).

Rechargeable lithium-ion batteries have been commercially successful energy storage devices dominating portable electronics. Electrodes in these batteries are based on intercalation reactions in which Li^+ ions are inserted (extracted) from an open host structure with electron addition (removal). Intercalation electrodes are successful because of the small structure and volume changes and fast Li^+ ion moving rate. However they have limited specific charge storage capacity and cannot meet the demands of higher energy density, higher power density, and longer lifespan for future portable electronics, power tools, electric and hybrid vehicles, and renewable energies. Recently, alloying reactions of elemental materials such as Si[1−10] and Sn[11−13] and conversion reactions of transition metal oxides[14,15] have been shown to offer specific charge storage capacity multiple times of the existing carbon anodes and to have great promises as future generation of battery electrodes. However, it is challenging to overcome the issues associated with alloying and conversion reactions, which involve large structure and volume changes during Li^+ ion insertion and extraction, and poor electron and ion conduction. These issues can cause large hysteresis in the charge and discharge potentials, low power rate, and short cycle life.

Exploiting nanostructured materials affords a promising means to address the challenges associated with alloying and conversion reactions because of the small diffusion length and the facile strain relaxation during structure and volume change. A variety of nanoparticles[3,16−18] and nanowires (NWs)[19−25] have been used as slurry randomly mixed with binder and conducting carbon for making battery electrodes and showed significant improvements. Designing nanoscale hierarchical structures is another effective way to address the issues associated with alloy and conversion electrodes. Martin and co-workers produced a new electrode configuration of active intercalation materials directly connected with a planar metal current collector using template synthesis.[26] Simon and co-workers developed this approach further by electrodepositing Cu nanorods to wire up conversion electrode materials.[15] Three-dimensional macroporous carbon has also been used to enhance lithium ion battery performance.[27] We have recently shown that an electrode configuration with single crystalline Si or Ge NWs grown directly on metal current collectors by vapor−liquid−solid (VLS) growth can offer good electrical connection and ability to overcome the mechanical breaking caused by up to 300% volume expansion.[28,29] Here we demonstrate a Si crystalline-amorphous

* To whom correspondence should be addressed. E-mail: yicui@stanford.edu.
[†] Department of Materials Science and Engineering, Stanford University.
[‡] Università degli Studi di Milano-Bicocca.
[§] Department of Chemistry, Stanford University.

10.1021/nl8036323 CCC: $40.75

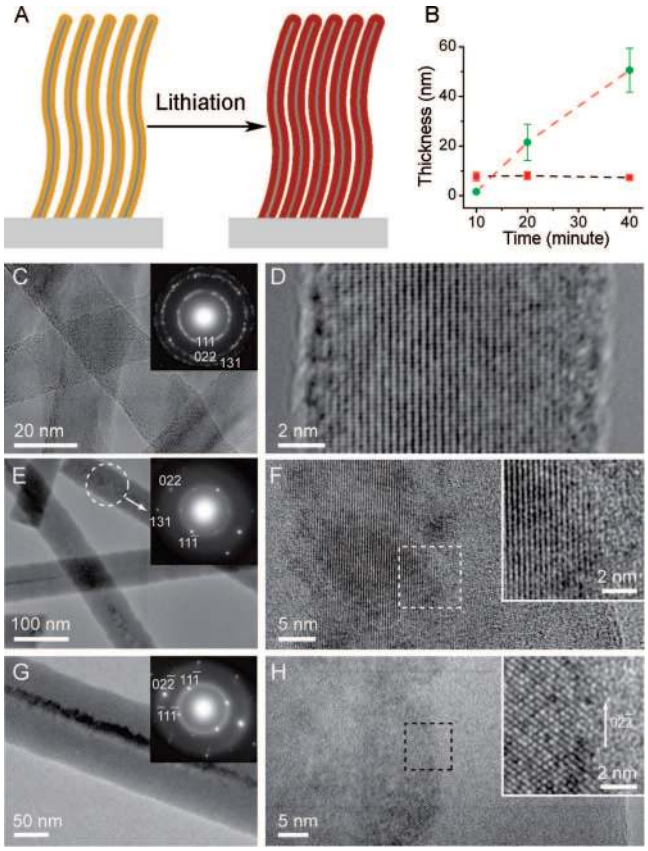

Figure 1. (A) Schematic illustration of the lithiation of the Si c-a core−shell NWs grown on a SS substrate. (B) Statistics of the core radius (red) and shell thickness (green) versus growth time. The growth temperature was 485 °C. (C) TEM and SAED images of NWs grown for 10 min. (D) HRTEM image of a NW grown for 10 min. (E) TEM and SAED images of NWs grown for 20 min. (F) HRTEM images of a NW grown for 20 min. (G) TEM and SAED images a NW grown for 40 min. (H) HRTEM images of a NW grown for 40 min.

(c-a) core−shell NW design resulting in significant improvement over power rate and cycling life.

Si is an alloying electrode material attracting much attention because of its highest known theoretical charge capacity. Both crystalline Si (c-Si) and amorphous Si (a-Si) can store Li^+ ions with similar specific capacity. Previous studies, mostly involving thin films, have suggested that a-Si has a superior cycling performance compared to c-Si.[30−32] One explanation for this is that the volume expansion of a-Si upon Li insertion is homogeneous and causes less pulverization as in the crystalline material.[30,33] Another interesting behavior of a-Si is that it reacts with lithium at slightly higher potential (∼220 mV)[4,31] than c-Si does (∼120 mV),[10,28] which leads to our idea of using c-a core−shell Si NWs as anode material. When limiting the charging potential, it should be possible to utilize only the amorphous shell material for Li^+ storage while preserving the crystalline core as mechanical support and efficient electron transport pathways, as indicated by Figure 1A.

Core−shell NWs for solar cells and transistors have been shown previously but not for batteries.[34−36] Lieber and coworkers have grown Au-catalyzed c-Si NWs in a chemical vapor deposition (CVD) furnace at 435 °C and coated a-Si shells at an elevated temperature of 450 °C.[37] Here we developed a simple method to grow c-a core−shell Si NWs without changing the growth condition. Our growth was conducted directly on stainless steel (SS) current collectors without Au as catalyst in a SiH_4 CVD furnace (see Materials and Methods, Supporting Information). We found that large flows, high pressure, and high temperatures promote the yield of c-a core−shell Si NWs on SS substrates (Supporting Information, Figure S1). Transition metals in SS, such as Fe, Ni, or Cr, are believed to catalyze the growth mostly likely by a direct vapor−solid (VS) mechanism since Fe and Ni have previously been shown to catalyze this kind of growth.[38−40] Figure 1B shows the statistics of the core radius and shell thickness versus growth time. Figure 1C−H shows the transmission electron microscopy (TEM) images and selected area electron diffraction (SAED) patterns of Si NWs grown at 485 °C for different growth time. For 10 min of growth, the NWs were mostly single crystalline (Figure 1C,D) with little amorphous shell. For 20 min, a thick layer of amorphous shell was observed (Figure 1E,F), which became even thicker for a 40 min growth (Figure 1G,H). As shown in Figure 1B, the thickness of amorphous shell is increased linearly with growth time while the core radius does not change. This suggests that c-Si cores were grown first and a-Si was subsequently coated onto the cores from SiH_4 decomposition. To confirm the amorphous shell is Si instead of SiO_2, we have measured energy dispersive X-ray spectroscopy (EDX), which shows dominantly Si signal with only trace amount of oxygen (Supporting Information, Figure S2). Since amorphous shell will be selectively used for Li^+ ion storage, an important question is what percentage of a-Si shells is in the c-a NWs. For the c-a NWs grown for 40 min, the a-Si shells dominate since they account for 98−99% by volume or weight. In our battery study, we used the c-a NWs grown for 40 min.

The c-a core−shell NWs were assembled into half-cells with Li metal as counter electrode (see Materials and Methods, Supporting Information). No binders or conducting carbon were used. The half-cells were studied using electrochemical potential spectroscopy (EPS)[41] and galvanostatic charge/discharge. In EPS measurement, a series of constant potential steps were applied to the electrochemical cell. On each step the cell was permitted to attain quasi equilibrium conditions by letting the current decay to a small but finite value (0.05C, typically ∼40 mA/g in our measurements). When small voltage steps (step size 5 mV in our study) were applied, the charge accumulated on each step were integrated from the measured current and yielded an accurate derivative of the voltage-charge relation. This derivative relation is a very useful tool to understand the structural transition inside electrode materials. In fact, under thermodynamic equilibrium condition the potential/composition profile obeys Gibbs phase rule,[41] that is, the potential is constant in a two-phase region but changes linearly in single-phase domain. So, the first derivative of quasi equilibrium charge/voltage curve can show sharp peaks for two-phase regions or bell-like peaks for single-phase regions, revealing whether a phase transformation occurs.

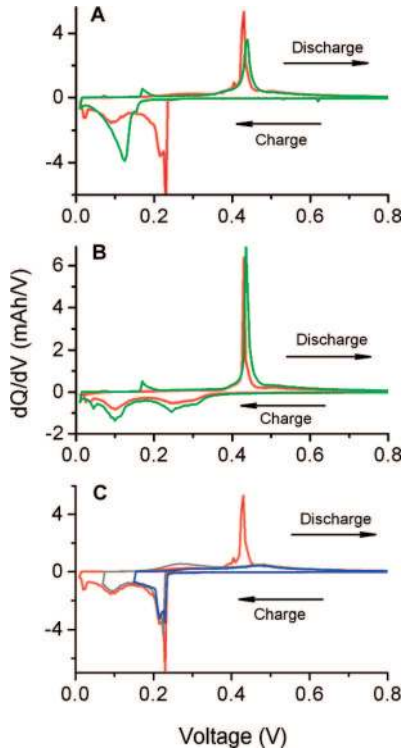

Figure 2. (A) Comparison of the first cycle EPS spectra of c-a core−shell NWs (red) and Au-catalyzed single crystalline NWs (green). (B) Comparison of the second cycle EPS spectra of core−shell NWs (red) and Au-catalyzed single crystalline NWs (green). (C) First cycle EPS spectra of core−shell NWs at different low voltage cutoffs of 10 mV (red), 70 mV (gray), and 150 mV (blue).

EPS was performed to study the behaviors of c-a NWs for the first and second cycles, which were compared with c-NWs grown by the Au-catalyzed VLS method. When the potential was stepped from 2 to 0.01 V during the first charge cycle (Figure 2A lower parts of the curves), c-a NWs show drastic difference from c-NWs. First, there is a sharp peak at 230 mV for c-a NWs but not for c-NWs, suggesting that the peak is due to the lithiation of the a-Si shell. The sharpness of this peak indicates the coexistence of two-phase structure of partially lithiated a-Si and unlithiated a-Si. Similar behavior has been suggested for c-Si powders by Obrovac et al.[4] This sharp peak also agrees with the previous thin film study on a-Si by Maranchi et al.[31] Second, at the potential range of 150−70 mV, the c-NWs show a sharp peak at 120 mV while the c-a NWs show a bell-like peak at a shifted potential of 100 mV. The sharp peak at 120 mV for c-NWs is attributed to the amorphorization of c-Si during the first lithiation process.[10,28] For the c-a NWs at 150−70 mV, lithiation of amorphous Li_xSi shell should be continued and also be accompanied by the amorphorization of c-Si core. The percentage of crystalline core material is too little (1−2 wt %) to contribute to the peak at 150−70 mV. Instead the peak is attributed to the further single-phase lithiation of amorphous Li_xSi shell, which explains its bell shape and shifted position.

For both c-a and c-NWs, further charging results in the formation of a new phase from amorphous Li_xSi at the peak potential of 40 mV. This new phase is likely due to crystalline $Li_{15}Si_4$, which was suggested by a previous study on Si powders and films.[4] Upon discharge (Figure 2A upper parts of the curves), both c-a and c-NWs show a sharp peak at 450 mV, indicating a transformation via coexistence of two phases of crystalline $Li_{15}Si_4$ and amorphous Li_xSi.[4] The small peak at 170 mV (Figure 2A, upper parts of the curves) for c-NWs is due to the delithiation of Au catalyst nanoparticles from the VLS growth, whose contribution is little and can be neglected. After the first cycle of charge and discharge between 2−0.01 V, both c-a and c-NWs turn into amorphous Li_xSi phase where x is very small.[10,28] During the second cycle bewteen 2−0.01V (Figure 2B), c-a NWs and c-NWs show similar behaviors. The two bell-shaped peaks (250 and 100 mV) during charge (Figure 2B, lower parts of the curves) are due to the lithiation of single-phase amorphous Li_xSi but with different site energies in the structure.

The above comparison of c-a and c-NWs suggests that it should be possible to cycle only the amorphous shell if the charge cutoff potential is maintained above the potential for amorphorization of c-Si (∼120 mV). Obrovac et al. have used a similar technique to preserve the crystalline cores of partially amorphorized Si particles.[4] To study the behavioral change when using different cutoffs, we have compared three c-a NW half-cells using EPS at the low-voltage cutoffs of 10 mV (red), 70 mV (gray), and 150 mV (blue) as shown in Figure 2C. Limiting the charge voltage above 70 mV prevents the formation of the crystalline $Li_{15}Si_4$ phase[4] and the successive discharge occurs in two single-phase regions shown by the two bell shape peaks (Figure 2C, gray curve) although the crystalline core can still be lithiated since the cutoff voltage is below 120 mV. With charge cutoff at 150 mV, the discharge happened mostly in just one single-phase region which corresponds to the broad bell-shape peak at 500 mV (Figure 2C upper part blue curve). In this case, the reaction involves just the external amorphous shell of the NWs and preserves the c-Si core for mechanical supports and efficient conductive pathways (See the structure characterization in Figure 4).

Now we compare the galvanostatic charge/discharge for c-a core−shell NWs with 10 and 150 mV cutoffs. For potential versus capacity plottings, see Figures S3 and S4 in Supporting Information. When a 10 mV cutoff was used, the whole NW would react with lithium to go through c-a phase transformation repeatedly and fatigue would occur. In Figure 3A, with a 10 mV cutoff and a current density of 0.85 A/g (0.2C according to the theoretical capacity of Si), the c-a core−shell NWs only retain 79% of the first discharge capacity after 30 cycles. The Coulombic efficiency is 80.4% for the first cycle and ∼98% between 5−30 cycles. In contrast, c-a core−shell NWs with a 150 mV cutoff and the same current density show dramatically improvement of cycle life (Figure 3B). The c-a NW electrode was charged to 150 mV in 1.2 h, showing a capacity of ∼1060 mAh/g with 85% discharge capacity retention over 100 cycles. Despite the discharge capacity of 150 mV cutoff is lower than that (2500 mAh/g) of 10 mV cutoff, the value is 3 times

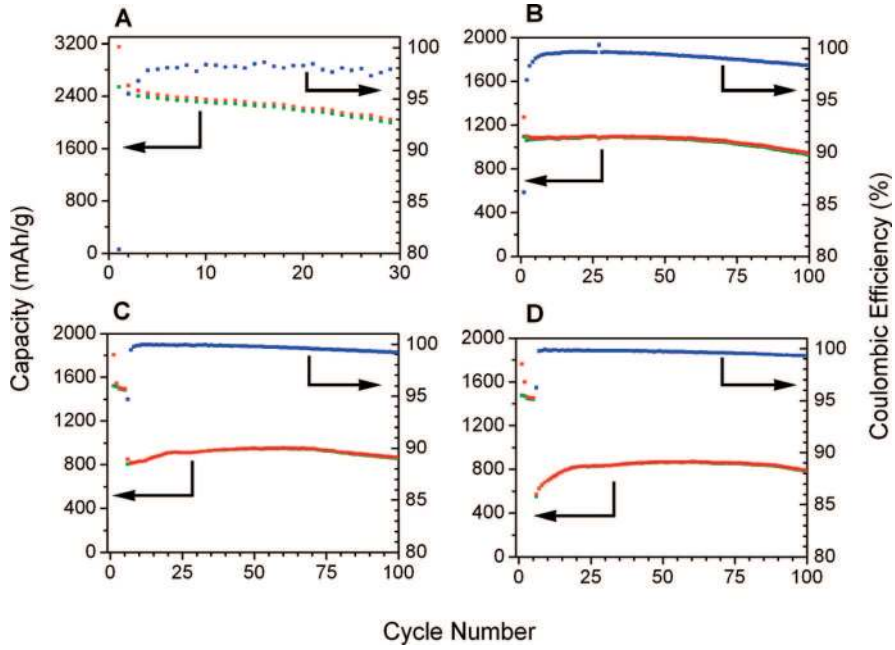

Figure 3. Charge (red) and discharge (green) capacity and Coulombic efficiency (blue) versus cycle number for the core−shell NWs with different low voltage cutoffs and power rates. (A) 10 mV cutoff and 0.2C (0.85 A/g). (B) 150 mV cutoff and 0.2C. (C) 150 mV cutoff, 0.1C for 5 cycles then 0.8C. (D) 150 mV cutoff, 0.1C for 5 cycles then 1.6C.

of carbon and is already high enough to be technologically significant. What is more important is to have good capacity retention over long cycle life. In addition, the Coulombic efficiency (86.2% for the first cycle, 99−99.7% for cycles 5−70, 98.4−99% for cycle 70−100) is significantly higher for the 150 mV cutoff, which provides a strong evidence of little fatigue of NWs during cycling.

A good mechanical support and efficient electron pathways in c-a core−shell NWs can also provide the opportunity for large current charge/discharge. Figure 3C,D shows the cycling performance of c-a core−shell NWs using a cutoff of 150 mV at higher power rates. Figure 3C shows the cycling performance of c-a NW electrode at 0.8C (3.4 A/g) rate till 100th cycle after operated at 0.1C rate for five cycles. Smaller rate of 0.1C was used at the beginning to condition the c-a NWs and expand the amorphous shell slowly. The discharge capacity at 0.8C starts with 807 mAh/g with a high Coulombic efficiency of 95%. The capacity increased gradually to 910 mAh/g at 20th cycle and retained 860 mAh/g after 100 cycles with little fading. The Coulombic efficiency (99.2−99.9%) is very high even with the fast 0.8C rate. Figure 3D shows the cycling performance of a NW electrode at an even higher rate of 1.6C (6.8 A/g) rate till 100th cycle. The capacity maintained a high value of ∼800 mAh/g and showed little fading after 100 cycles. High Coulombic efficiencies (99.3−99.9%) were observed as well. We noted that it only took 7 min to charge/discharge the Si NW anode at 1.6C rate. This completely off-scale of time is due to the significant lower capacity compared to the theoretical capacity of Si. Our actual specific current density is extremely high, equivalent to only ∼2 min charge/discharge rate in graphite anode.

To confirm that the c-a core−shell structure still remained for robust mechanical and electrical support after cycling,

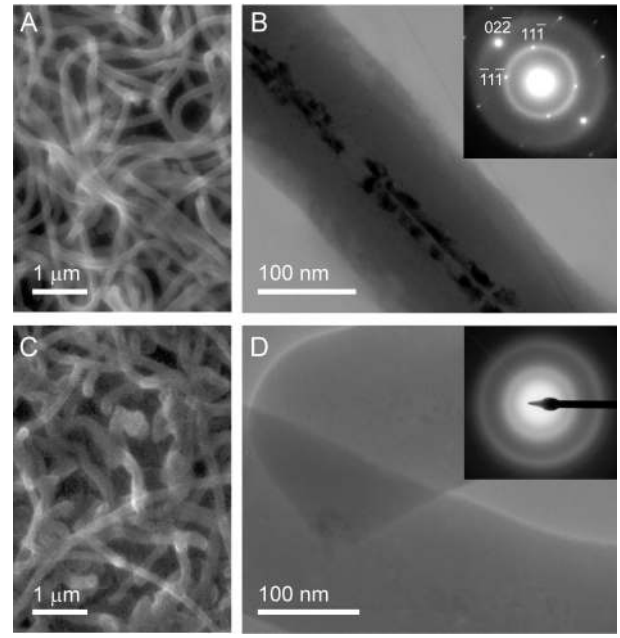

Figure 4. SEM, TEM, and SAED images of the c-a core−shell NWs after cycling at 0.2C (0.85 A/g) and different low voltage cutoffs. (A) SEM image of NWs after 15 cycles with cutoff of 150 mV. (B) TEM and SAED (inset) images of a NW after 15 cycles with cutoff of 150 mV. (C) SEM image of NWs after 3 cycles with cutoff of 10 mV. (D) TEM and SAED (inset) images of NWs after 3 cycles with cutoff of 10 mV.

we have investigated the morphology and structure of cycled c-a NWs (delithiated at the end of cycling) with scanning electron microscopy (SEM) and TEM. Two samples cycled with 150 and 10 mV cutoffs are compared in Figure 4. Figure 4A shows the SEM image of the c-a core−shell NWs after 15 cycles using a 150 mV cutoff, where the NWs apparently still maintain good wire shapes. Figure 4B shows the TEM

image of a corresponding single NW, which still clearly shows a core−shell structure by contrast. SAED pattern (Figure 4B inset) confirms that the core is still crystalline Si. The bright and dark contrast of crystalline Si core might be caused by the straining effect of the expansion of amorphous shell during lithium insertion. Figure 4C shows the SEM image of the c-a core−shell NWs after 3 cycles using a cutoff of 10 mV. Figure 4D is the TEM image and SAED pattern (inset) of corresponding NWs, indicating a complete amorphous structure without crystalline core. This was well expected since the crystalline core would react with lithium at 10 mV and become totally amorphous upon cycling, which was also indicated by previous studies.[10,28]

In conclusion, we have grown silicon crystalline-amorphous core−shell nanowires on stainless steel substrates using a simple one-step synthesis. Amorphous Si shells instead of crystalline Si cores can be selected to be electrochemically active due to the difference of their lithiation potentials. Therefore, crystalline Si cores function as a stable mechanical support and an efficient electrical conducting pathway while amorphous shells store Li^+ ions. We demonstrate that these core−shell nanowires have high charge storage capacity (∼1000 mAh/g, 3 times of carbon) with ∼90% capacity retention over 100 cycles. They also show excellent electrochemical performance at high rate of charging and discharging (6.8 A/g, ∼20 times of carbon at 1 h rate).

Acknowledgment. Y.C. acknowledges support from the Global Climate and Energy Project at Stanford, U.S. Office of Naval Research and King Abdullah University of Science and Technology. C.K.C. acknowledges support from a National Science Foundation graduate fellowship and Stanford Graduate Fellowship.

Supporting Information Available: Detailed experimental method, SEM images, EDX spectra, and charge−discharge potential profiles. This material is available free of charge via the Internet at http://pubs.acs.org.

References

(1) Winter, M.; Besenhard, J. O.; Spahr, M. E.; Novak, P. *Adv. Mater.* **1998**, *10* (10), 725–763.
(2) Beaulieu, L. Y.; Hatchard, T. D.; Bonakdarpour, A.; Fleischauer, M. D.; Dahn, J. R. *J. Electrochem. Soc.* **2003**, *150* (11), A1457−A1464.
(3) Kasavajjula, U.; Wang, C. S.; Appleby, A. J. *Journal of Power Sources* **2007**, *163* (2), 1003–1039.
(4) Obrovac, M. N.; Krause, L. J. *J. Electrochem. Soc.* **2007**, *154* (2), A103−A108.
(5) Yang, J.; Winter, M.; Besenhard, J. O. *Solid State Ionics* **1996**, *90* (1−4), 281–287.
(6) Kim, J. W.; Ryu, J. H.; Lee, K. T.; Oh, S. M. *J. Power Sources* **2005**, *147* (1−2), 227–233.
(7) Boukamp, B. A.; Lesh, G. C.; Huggins, R. A. *J. Electrochem. Soc.* **1981**, *128* (4), 725–729.
(8) Hatchard, T. D.; Dahn, J. R. *J. Electrochem. Soc.* **2004**, *151* (6), A838−A842.
(9) Obrovac, M. N.; Christensen, L. *Electrochem. Solid-State Lett.* **2004**, *7* (5), A93−A96.
(10) Limthongkul, P.; Jang, Y. I.; Dudney, N. J.; Chiang, Y. M. *Acta Mater.* **2003**, *51* (4), 1103–1113.
(11) Mao, O.; Dunlap, R. A.; Dahn, J. R. *J. Electrochem. Soc.* **1999**, *146* (2), 405–413.
(12) Winter, M.; Besenhard, J. O. *Electrochim. Acta* **1999**, *45* (1−2), 31–50.
(13) Beaulieu, L. Y.; Dahn, J. R. *J. Electrochem. Soc.* **2000**, *147* (9), 3237–3241.
(14) Poizot, P.; Laruelle, S.; Grugeon, S.; Dupont, L.; Tarascon, J. M. *Nature* **2000**, *407* (6803), 496–499.
(15) Taberna, P. L.; Mitra, S.; Poizot, P.; Simon, P.; Tarascon, J. M. *Nat. Mater.* **2006**, *5* (7), 567–73.
(16) Ryu, J. H.; Kim, J. W.; Sung, Y. E.; Oh, S. M. *Electrochem. Solid-State Lett.* **2004**, *7* (10), A306−A309.
(17) Mao, O.; Turner, R. L.; Courtney, I. A.; Fredericksen, B. D.; Buckett, M. I.; Krause, L. J.; Dahn, J. R. *Electrochem. Solid-State Lett.* **1999**, *2* (1), 3–5.
(18) Kim, I. S.; Kumta, P. N. *J. Power Sources* **2004**, *136* (1), 145–149.
(19) Nam, K. T.; Kim, D. W.; Yoo, P. J.; Chiang, C. Y.; Meethong, N.; Hammond, P. T.; Chiang, Y. M.; Belcher, A. M. *Science* **2006**, *312* (5775), 885–888.
(20) Shaju, K. M.; Jiao, F.; Debart, A.; Bruce, P. G. *Phys. Chem. Chem. Phys.* **2007**, *9* (15), 1837–1842.
(21) Park, M. S.; Wang, G. X.; Kang, Y. M.; Wexler, D.; Dou, S. X.; Liu, H. K. *Angew. Chem., Int. Ed.* **2007**, *46* (5), 750–753.
(22) Armstrong, G.; Armstrong, A. R.; Bruce, P. G.; Reale, P.; Scrosati, B. *Adv. Mater.* **2006**, *18* (19), 2597.
(23) Kim, D. K.; Muralidharan, P.; Lee, H. W.; Ruffo, R.; Yang, Y.; Chan, C. K.; Peng, H. L.; Huggins, R. A.; Cui, Y. *Nano Lett.* **2008**, *8*, 3948–3952.
(24) Li, Y. G.; Tan, B.; Wu, Y. Y. *Nano Lett.* **2008**, *8* (1), 265–270.
(25) Lou, X. W.; Deng, D.; Lee, J. Y.; Feng, J.; Archer, L. A. *Adv. Mater.* **2008**, *20*, 258–262.
(26) Li, N. C.; Martin, C. R. *J. Electrochem. Soc.* **2001**, *148* (2), A164−A170.
(27) Lee, K. T.; Lytle, J. C.; Ergang, N. S.; Oh, S. M.; Stein, A. *Adv. Funct. Mater.* **2005**, *15* (4), 547–556.
(28) Chan, C. K.; Peng, H. L.; Liu, G.; McIlwrath, K.; Zhang, X. F.; Huggins, R. A.; Cui, Y. *Nat. Nanotechnol.* **2008**, *3*, 31–35.
(29) Chan, C. K.; Zhang, X. F.; Cui, Y. *Nano Lett.* **2008**, *8*, 307–309.
(30) Yin, J. T.; Wada, M.; Yamamoto, K.; Kitano, Y.; Tanase, S.; Sakai, T. *J. Electrochem. Soc.* **2006**, *153* (3), A472−A477.
(31) Maranchi, J. P.; Hepp, A. F.; Kumta, P. N. *Electrochem. Solid-State Lett.* **2003**, *6* (9), A198−A201.
(32) Ohara, S.; Suzuki, J. J.; Sekine, K.; Takamura, T. *Electrochemistry* **2003**, *71* (12), 1126–1128.
(33) Beaulieu, L. Y.; Eberman, K. W.; Turner, R. L.; Krause, L. J.; Dahn, J. R. *Electrochem. Solid-State Lett.* **2001**, *4* (9), A137−A140.
(34) Tian, B. Z.; Zheng, X. L.; Kempa, T. J.; Fang, Y.; Yu, N. F.; Yu, G. H.; Huang, J. L.; Lieber, C. M. *Nature* **2007**, *449*, 885–U8.
(35) Goldberger, J.; Hochbaum, A. I.; Fan, R.; Yang, P. D. *Nano Lett.* **2006**, *6* (5), 973–977.
(36) Bryllert, T.; Wernersson, L. E.; Froberg, L. E.; Samuelson, L. *IEEE Electron Device Lett.* **2006**, *27* (5), 323–325.
(37) Dong, Y. J.; Yu, G. H.; McAlpine, M. C.; Lu, W.; Lieber, C. M. *Nano Lett.* **2008**, *8*, 386–391.
(38) Liu, Z. Q.; Xie, S. S.; Zhou, W. Y.; Sun, L. F.; Li, Y. B.; Tang, D. S.; Zou, X. P.; Wang, C. Y.; Wang, G. *J. Cryst. Growth* **2001**, *224* (3−4), 230–234.
(39) Li, C.; Gu, C.; Liu, Z. T.; Mi, J. X.; Yang, Y. *Chem. Phys. Lett.* **2005**, *411* (1−3), 198–202.
(40) Chen, X. H.; Xing, Y. J.; Xu, J.; Xiang, J.; Yu, D. P. *Chem. Phys. Lett.* **2003**, *374* (5−6), 626–630.
(41) Thompson, A. H. *J. Electrochem. Soc.* **1979**, *126* (4), 608–616.

NL8036323